Supporting Information

Menon et al. 10.1073/pnas.0901783106

SI Text

Histidine-Tagged DC-SIGN (His_6-DC-SIGN) Expression and Purification. A previously described vector for bacterial expression of the extracellular domain of human DC-SIGN (1) was modified to incorporate sequences encoding an N-terminal His_6 tag. Insertion of a synthetic double-stranded oligonucleotide to place the sequence ggatccgatcttggaggatgattaaatggcccaccatcaccatcatcacggtgagctc between the BamH1 site in the vector and a SacI site near the 3′ end of the cDNA sequence resulted in a vector encoding the sequence Met-Ala-His-His-His-His-His-His-Gly-Glu-Leu, which begins at residue 101 of the full-length DC-SIGN protein, corresponding to the middle of the first 23-aa repeat in the extracellular domain. The tagged protein was purified by affinity chromatography on mannose-Sepharose following the protocol used for the untagged extracellular domain (1).

$Man_9GlcNAc_2$-DPPE Preparation and Purification. Soybean agglutinin was purified by affinity chromatography on immobilized *N*-acetylgalactosamine (2). The $Man_9GlcNAc_2$ oligosaccharide was released by hydrazinolysis (3) and assayed by using the anthrone method (4). The $Man_9GlcNAc_2$-DPPE conjugate (Fig. S1) was prepared by using sodium cyanoborohydride by published procedures (5) that were scaled up so that 5 mg of lyophilized oligosaccharide was reacted with 100 mg of DPPE. For purification, dried aliquots from the reaction were suspended in 1.5 mL of solvent G (water/methanol/chloroform, 6:14:3) and applied to a 1-mL C18 cartridge (Sep-Pak; Waters) that was rinsed with 0.5 mL of solvent G and eluted with 7 0.3-mL aliquots of solvent G. High-performance silica gel thin-layer chromatography was used to identify fractions containing neoglycolipid but not free lipid. A total of 100–200 μg of $Man_9GlcNAc_2$-DPPE (Fig. S1) was obtained from the original reaction.

Langmuir–Blodgett Deposition of Asymmetric Supported Bilayers. Both the NTA-TRIG-DLGE and the neoglycolipid monolayers were supported on gel-phase DPPE monolayers on mica sheets. The resulting asymmetric, planar lipid bilayers were prepared by Langmuir–Blodgett deposition, as described previously (6). To deposit the gel-phase DPPE monolayer on the mica, a 9:1 chloroform/methanol DPPE solution was spread dropwise on the water surface of the subphase in the Langmuir trough (Nima), and the solvent was allowed to evaporate. The lipid molecules, being amphiphilic, orient at the air–water interface with head groups in the aqueous subphase and hydrophobic tails in the air. The lipid composition in the spread solution determines the composition of the lipid monolayer. A Teflon barrier is then moved across the water surface to confine the lipids to a defined area and thereby to control the molecular packing. The amount of lipid spread on the subphase surface is known, so the average area per lipid molecule can be determined from the confinement area divided by the number of lipid molecules. The lipid packing density determines the surface pressure of the lipid monolayer, as measured with a Wilhelmy balance (Nima).

To deposit DPPE onto mica, the DPPE monolayer is first compressed to 43 Å^2 per lipid molecule, as assessed by the measured surface pressure. The compressed monolayer is transferred to the mica surface by pulling the mica vertically up through the air–water interface at constant surface pressure and dipping speed. The DPPE molecules transfer onto the mica with head groups adjacent to the mica and close-packed tails exposed to the air. To form the second, outer layer, the fluid NTA-TRIG-DLGE or mixed DTPC: $Man_9GlcNAc_2$-DPPE lipids are similarly spread on the air-water interface, the monolayer is compressed to ≈65 Å^2 per lipid. The second layer is transferred onto the DPPE monolayer by dipping the supported DPPE monolayer vertically into the subphase. The second lipid monolayer transfers onto the DPPE with the tails adjacent to the DPPE and the head groups exposed to the aqueous subphase. These supported bilayers are kept under water at all times.

Quantifying Force–Distance Profiles in Surface Force Apparatus Measurements. The surface force apparatus quantifies the net force (F) between macroscopic surfaces. In the surface force apparatus measurements, the samples are supported on 2 macroscopic lenses whose surfaces are polished hemicylinders with radii of curvature of 1–2 cm. The cylinders are oriented perpendicular to each other in the apparatus. The measurements then quantify the net force F between the cylinders normalized by their geometric average radius (R), as a function of the absolute separation distance D (7, 8). The crossed-cylinder geometry is equivalent to a flat plate interacting with a sphere with a radius equal to the geometric mean of the radii of the 2 hemicylinders. The thus normalized force (F/R) is directly proportional to the energy per area between equivalent flat plates (9). The absolute distances are determined within ±0.1 nm by interferometry (10). The forces are measured both during the approach and separation of the 2 surfaces.

The instrument quantifies either repulsive (branch A → B, Fig. S2) or attractive forces (branches C → D and D → E → F, Fig. S2). In the case of intersurface repulsion ($F > 0$), when the 2 surfaces are brought into contact, the force field causes the disk attached to the spring (force transducer) to deflect away from the substrate by an amount ΔD_c (Fig. S2). From the spring constant k_c, Hooke's Law gives the normalized intersurface repulsive force $F/R = k_c\Delta D_c/R$ at the absolute probe–surface distance at point B on the curve. Measurements of the force at several distances along the A–B branch map the normalized force versus distance profile.

In the case of attractive forces ($F < 0$), the magnitude of the adhesion (net attractive force relative to $F = 0$) is determined upon surface separation from the force required to pull the surfaces out of adhesive contact and is designated the pull-off force F_{Adh}. This is the maximum attractive force. The distance at pull-off, D_{Adh}, is the position at which the maximum attractive force is measured (point E, Fig. S2). This is also the position of the maximum gradient in the intersurface potential. In the case of the crossed-cylinder sample geometry used in the surface force apparatus experiments, F_{Adh} between the crossed-cylinders is related to the adhesion energy per area between equivalent flat plates E_f by the Derjaguin–Müller–Toporov theory (9): $E_f = F_{Adh}/2\pi R$, where R is the geometric mean radius of the crossed cylinders. This equation directly relates the adhesive force between undeformed, curved surfaces to the adhesion energy per area between 2 flat surfaces of identical composition.

In some cases, the surfaces spontaneously jump in to adhesive contact [upper right (arrow pointing "in"); Fig. S2). This occurs from a distance D_J, where the gradient of the intersurface potential exceeds the spring constant (6). After the jump, the surfaces come to rest at the equilibrium distance D_{eq} (point C in Fig. S2). In the case of receptors and ligands, D_{eq} is determined by the thickness of the receptor–ligand complex (T_1 and T_2, see illustrations corresponding to points A and C in Fig. S2): the receptor–ligand adhesion holds the surfaces together, but the thickness of the complex determines the intersurface separation,

in the absence of any externally applied compressive force. The surfaces may pull out of contact at distances D_{Adh} that are $>D_{eq}$ if the molecules rearrange under a tensile (stretching) force.

Determining the Equilibrium Adhesion Energies as a Function of Ligand Density. In the adhesion measurements, some CRDs and ligands will not be in register when the surfaces initially come into contact, but the ligands in fluid membranes can diffuse to unoccupied CRDs. The idea that lateral diffusion of ligands enables the engagement of multiple CRDs is consistent with the fact that the DC-SIGN adhesion to $Man_9GlcNAc_2$-DPPE in fluid membranes depends on the contact time between the surfaces (Fig. S3*A*). As observed previously with other receptors (11, 12), increased contact times allow time for the ligands to undergo rotational and translational diffusion to engage with DC-SIGN CRDs. In contrast, the time-dependent change in adhesion with gel-phase membranes is small (Fig. S3*B*) and is attributed to the more limited lateral mobility of the DC-SIGN, which is immobilized on a fluid lipid membrane.

During the period that ligands are equilibrating with the opposing CRDs, the adhesion energy increases with time, until ligands and CRDs achieve an equilibrated distribution of bound and free states. To quantify the equilibrium adhesion energy at different ligand concentrations, the adhesion time courses were fitted, using nonlinear regression, to the empirical functions:

$$E_{eq} = \alpha_1(1 - \exp^{-\beta_1 t}) \qquad \textbf{[s1]}$$

and

$$E_{eq} = \alpha_1(1 - \exp^{-\beta_1 t}) + \alpha_2(1 - \exp^{-\beta_2 t}) \qquad \textbf{[s2]}$$

The fitted parameters are given in Table S1. The prefactor α is the adhesion energy, extrapolated to $t \rightarrow \propto$, and $1/\beta$ is the time to reach 63% of the maximum adhesion. This adhesion energy per area extrapolated to the limiting plateau is assumed to be the equilibrium adhesion energy. The fitted prefactor α characterizes the limiting adhesion energy—assumed to be the equilibrium adhesion energy. This depends on the ligand density and mobility. Eq. **s1** better describes the time-dependent adhesion at ligand densities less than 5 mol %. However, at ≥5 mol %, there is an initial fast binding that is followed by a slower increase to a limiting plateau. An F test confirmed that the latter behavior is better described by 2 exponentials (Eq. **s2**). Thus, binding is a 2-step process, in which the initial fast reaction is described by (α_1, β_1), and the latter slower second step is described by (α_2, β_2). At time $t \rightarrow \propto$, the equilibrium adhesion energy is given by $\alpha_1 + \alpha_2$.

This difference in behavior at low and high ligand densities can be explained by differences in the timing of multiple CRD engagement with multiple ligand molecules. At the lowest ligand densities, DC-SIGN likely only encounters a single ligand on initial intersurface contact, such that the subsequent diffusion-controlled ligand binding to equilibrium occupancy generates the single exponential rise to the limiting plateau. The biphasic time dependence of the adhesion at higher $Man_9GlcNAc_2$-DPPE densities would reflect the fact that under these conditions, multiple bonds form rapidly upon initial contact, resulting in a higher initial adhesion. The subsequent rise is due to diffusion-controlled ligand binding to the remaining unoccupied CRDs.

Determination of DC-SIGN Surface Coverage. A home-built surface plasmon resonance instrument (13) was used to quantify the amount of DC-SIGN immobilized on the supported lipid bilayers. Substrates consisted of a clean glass slide, which was coated with a chromium adhesion layer (2 nm), followed by a 39-nm-thick layer of gold. The metal films were deposited by thermal evaporation at a pressure of 5×10^{-6} Pa. The gold-coated slide was then immersed in a 0.5 mM ethanolic solution of 1-octadecanethiol and incubated overnight at room temperature, to form a self-assembled alkanethiol monolayer. The hydrophobic surface was coated with a monolayer of 100% NTA-TRIG-DLGE by Langmuir–Blodgett deposition. The lipid monolayer was transferred at the constant pressure of 35 mN/m from Buffer A. The sample was then assembled in the surface plasmon resonance cell.

To measure specific DC-SIGN adsorption, after flushing the flow cell with running buffer (20 mM Hepes, 50 mM $NaNO_3$, 3 mM $Ca(NO_3)_2$, and 50 μM $NiSO_4$ at pH 7.8) for 25 min, 1 mL of 0.5 μM DC-SIGN was injected into the cell and left to incubate for 1.5 h. This is the incubation time used for all of the surface force experiments in this study. During this time, the protein adsorption was tracked by the change in the plasmon resonance angle. Afterward, the cell was flushed with running buffer to remove nonspecifically bound DC-SIGN.

The effective optical thickness of the adsorbed protein layer was determined by fitting the resonance curves to Fresnel equations for a multilayer film with a 5-phase Fresnel program obtained from R. Corn (University of California, Irvine). The effective optical thickness is the product of the refractive index and thickness of the protein monolayer. The DC-SIGN surface coverage was calculated from the optical thickness by using 32.8 nm as the measured DC-SIGN thickness and 1.46 as the refractive index of the protein. The latter constants were both determined with the surface force apparatus. The surface coverage of DC-SIGN was thus calculated to be $8.5 \pm 0.2 \times 10^{11}$ molecules per cm^2.

1. Mitchell DA, Fadden AJ, Drickamer K (2001) A novel mechanism of carbohydrate recognition by the C-type lectins DC-SIGN and DC-SIGNR. Subunit organization and binding to multivalent ligands. *J Biol Chem* 276:28939–28945.
2. Gordon J, Blumberg S, Lis H, Sharon N (1972) Purification of soybean agglutinin by affinity chromatography On sepharose-*N*-epsilon-aminocaproyl-beta-D-galactopyranosylamine. *FEBS Lett* 24:193–196.
3. Ashford D, et al. (1987) The beta 1–2-D-xylose and alpha 1–3-L-fucose substituted *N*-linked oligosaccharides from *Erythrina cristagalli* lectin. Isolation, characterisation and comparison with other legume lectins. *Eur J Biochem* 166:311–320.
4. Spiro R (1966) Analysis of sugars found in glycoproteins. *Methods Enzymol* 8:1–26.
5. Feizi T, Childs R (1994) Neoglycolipids: probes in structure/function assignments to oligosaccharides. *Methods Enzymol* 242:205–217.
6. Marra J, Israelachvili J (1985) Direct measurements of forces between phosphatidylcholine and phosphatidylethanolamine bilayers in aqueous electrolyte solutions. *Biochemistry* 24:4608–4618.
7. Leckband D, Israelachvili J (2001) Intermolecular forces in biology. *Q Rev Biophys* 34:105–267.
8. Israelachvili J, Adams G (1978) Measurement of forces between two mica surfaces in aqueous electrolyte solutions in the range 0–100 nm. *J Chem Soc Faraday Trans I* 75:975–1001.
9. Israelachvili J (1992) *Intermolecular and Surface Forces* (Academic, New York).
10. Israelachvili J (1973) Thin film studies using multiple-beam interferometry. *J Colloid Interface Sci* 44:259–272.
11. Bayas M, et al. (2007) Impact of salt bridges on the equilibrium binding and adhesion of human CD2 and CD58 *J Biol Chem* 282:5589–5596.
12. Leckband D, Schmitt F, Israelachvili J, Knoll W (1994) Direct force measurements of specific and nonspecific protein interactions. *Biochemistry* 33:4611–4624.
13. Lavrik N, Leckband D (2000) Optical and direct force measurements of the interaction between monolayers of aromatic macrocycles on surfactant monolayers. *Langmuir* 16:1842–1851.

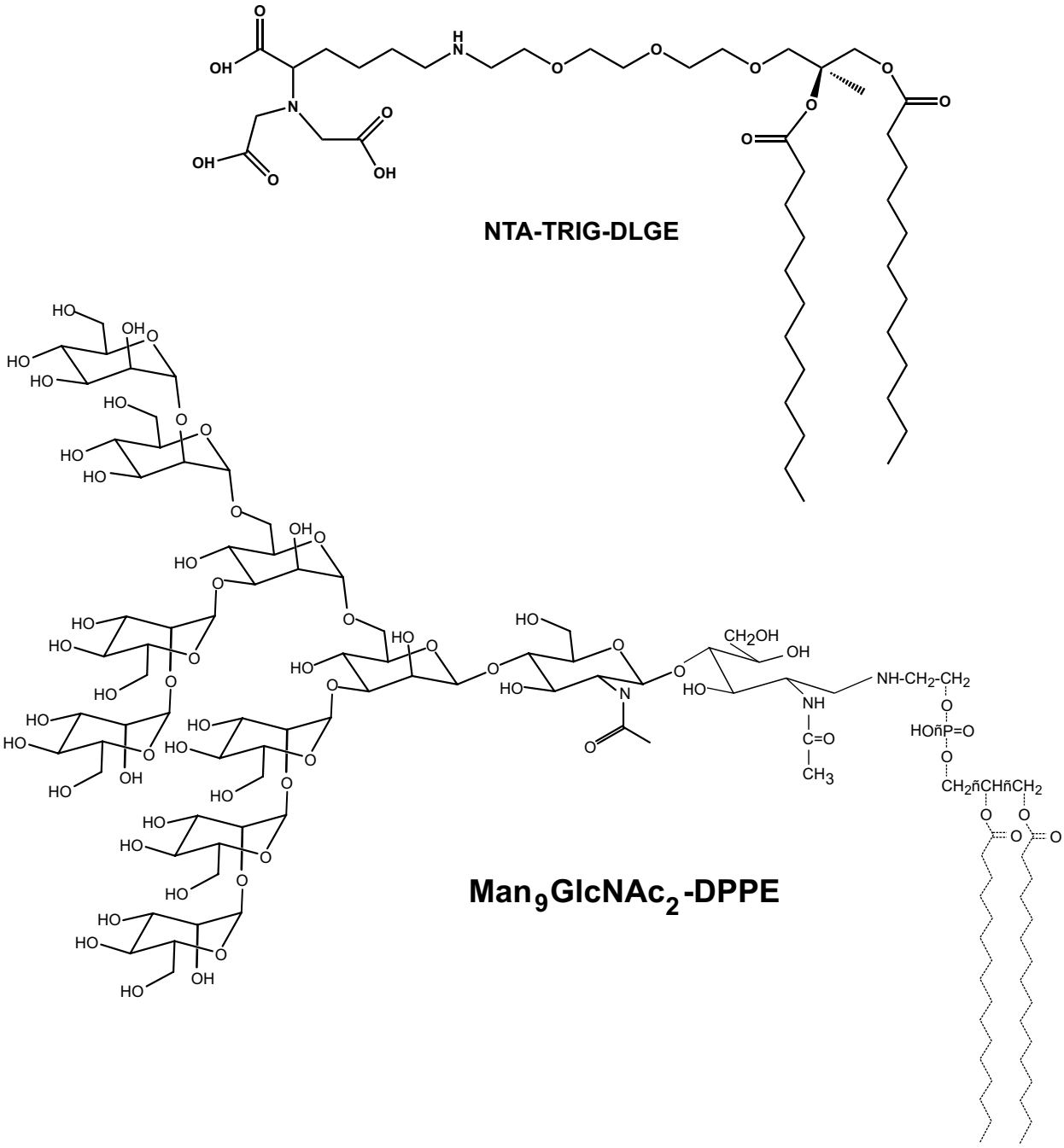

Fig. S1. Chemical structure of the NTA-Trig-DLGE lipid and of the $Man_9GlcNAc_2$-DPPE neoglycolipid.

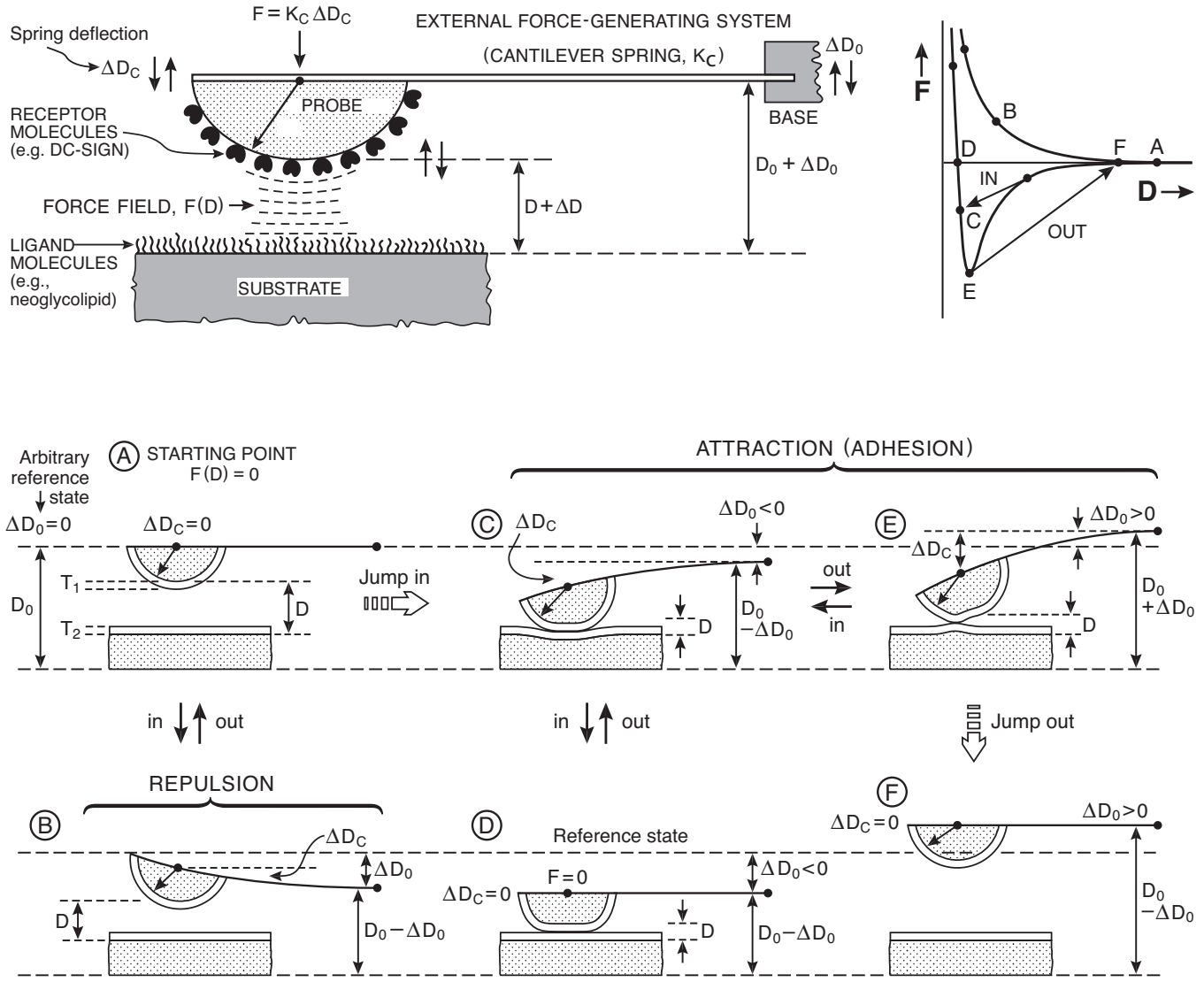

Fig. S2. Principles of the surface force apparatus measurements. (*Upper Left*) The probe surface, with an average radius of R, coated with receptor (DC-SIGN) molecules of thickness T_1 (*A*). The substrate is coated with ligand (neoglycolipid) molecules of thickness T_2 (*A*). An external force-generating system that consists of a cantilever with a spring constant K_C is controlled by an external positioning control system, which moves the probe relative to an initial position D_0 by a distance $\pm\Delta D_0$. The cantilever movement causes the distance D between the probe tip and substrate to shift by $\pm\Delta D$. The deflection of the spring, caused by the force field between the surfaces $F(D)$, is determined from Hooke's Law: $F(D) = K_C\Delta D_C$. (*Upper Right*) Two force-distance curves are shown. (A–F) The corresponding probe positions and spring deflections are indicated. Beginning from D_0 at point A on the force–distance curve, the cantilever moves toward the surface by $-\Delta D_0$. If the force is repulsive (*B*), then the probe deflects away from the surface by ΔD_C, which is proportional to the probe–substrate force at the distance corresponding to B on the force–distance curve (*Upper Right*). If the surfaces attract, then the probe may jump into contact (*C*), causing the cantilever to deflect toward the substrate. This deflection gives the attractive force at point C on the force–distance plot. The cantilever moves toward the substrate by $-\Delta D_0$ to (*D*), such that the net force on the cantilever is zero (position D on force–distance curve). When the cantilever moves away from the substrate by $+\Delta D_0$, the surfaces adhere, so that the spring deflects ΔD_C in the opposite direction. (*E*) The spring deflects by the maximum amount, which gives the magnitude of the attractive force at point E on the force–distance curve. (*F*) The bonds then fail, and the surfaces jump out of contact and come to rest at position F on the force–distance curve.

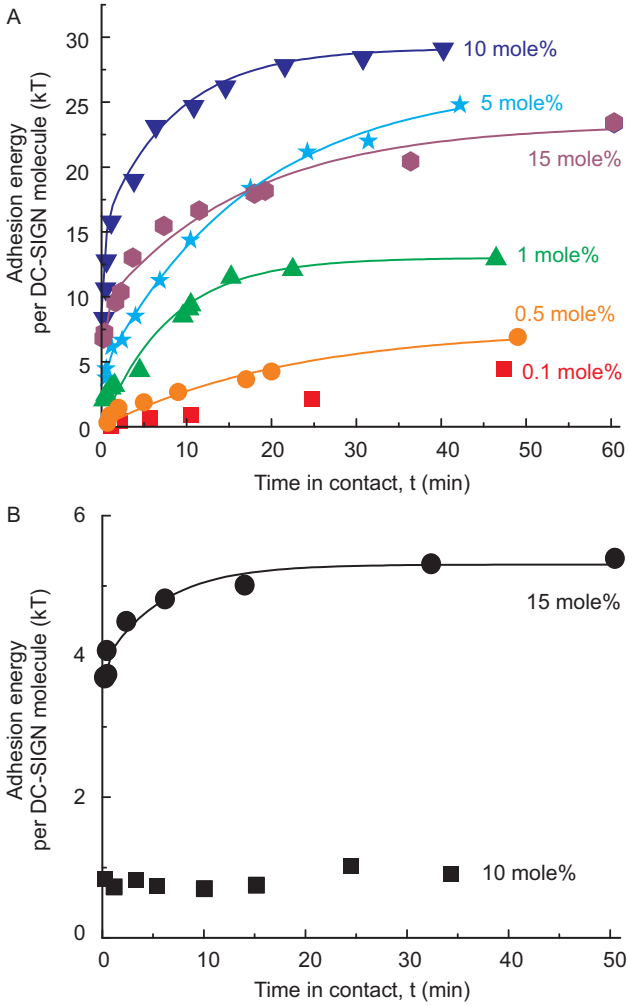

Fig. S3. Dependence of adhesion between membranes displaying DC-SIGN and $Man_9GlcNAc_2$-DPPE on the intersurface contact time. The contact time is defined as the time from when the surfaces jump into contact to the time at pull off. (*A*) Adhesion measured with fluid membranes. (*B*) Adhesion measured with gel membranes. The solid lines through the data are fits to empirical functions (Eqs. **s1 and s2**), and the fitted parameters are given in Table S1.

Table S1. Nonlinear regression of adhesion energy as a function of contact time

	$Man_9GlcNAc_2$-DPPE density, mol %	α_1	β_1	α_2	β_2	R^2	Equilibrium adhesion
Fluid	0.01	–	–	–	–	–	0
	0.1	–	–	–	–	–	4.5 ± 0.7*
	0.5	7.6 ± 1.0	0.05 ± 0.01	–	–	0.96	7.6 ± 0.6
	1	13.0 ± 0.9	0.13 ± 0.02	–	–	0.94	13.0 ± 0.7
	5	22.3 ± 0.8	0.06 ± 0.01	4.3 ± 0.5	3.3 ± 1.3	0.99	26.6 ± 1.3
	10	14.4 ± 1.0	0.1 ± 0.02	14.4 ± 1.0	2.6 ± 0.4	0.99	28.8 ± 1.4
	15	14.1 ± 1.3	0.06 ± 0.02	9.2 ± 0.9	5.1 ± 1.6	0.97	23.3 ± 1.2
Gel	0.01	–	–	–	–	–	0
	0.5	–	–	–	–	–	0
	5	–	–	–	–	–	0
	10	–	–	–	–	–	0.8 ± 0.4†
	15	3.9 ± 0.2	12.3 ± 4.7	1.4 ± 0.2	0.2 ± 0.1	0.96	5.3 ± 0.6

*The fit to Eq. **s1** does not converge for this density, and the value quoted is the maximum adhesion for maximum contact time reported.
†Adhesion is constant over time, and hence, it is the average of all the values obtained over time.